JACS
JOURNAL OF THE AMERICAN CHEMICAL SOCIETY
Article
pubs.acs.org/JACS

Solution Voltammetry of 4 nm Magnetite Iron Oxide Nanoparticles

Joseph J. P. Roberts, John A. Westgard, Laura M. Cooper, and Royce W. Murray*

Department of Chemistry, University of North Carolina, Chapel Hill, North Carolina 27599, United States

Supporting Information

ABSTRACT: The voltammetry of solution-dispersed magnetite iron oxide Fe_3O_4 nanoparticles is described. Their currents are controlled by nanoparticle transport rates, as shown with potential step chronoamperometry and rotated disk voltammetry. In pH 2 citrate buffer with added $NaClO_4$ electrolyte, solution cyclic voltammetry of these nanoparticles (average diameter 4.4 ± 0.9 nm, each containing ca. 30 Fe sites) displays an electrochemically irreversible oxidation with E_{PEAK} at ca. +0.52 V and an irreversible reduction with E_{PEAK} at ca. +0.2 V vs Ag/AgCl reference electrode. These processes are presumed to correspond to the formal potentials for one-electron oxidation of Fe(II) and reduction of Fe(III) at their different sites in the magnetite nanoparticle structure. The heterogeneous electrode reaction rates of the nanoparticles are very slow, in the 10^{-5} cm/s range. The nanoparticles are additionally characterized by a variety of tools, e.g., TEM, UV/vis, and XPS spectroscopies.

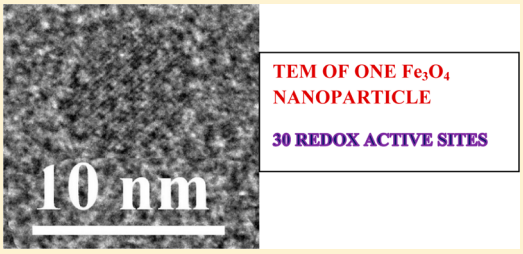

INTRODUCTION

Magnetic iron oxide nanoparticles and solutions thereof are significant nanomaterials, having technological applications in data storage and improved electronic devices.[1] They are also an active topic in medical areas[2−4] given their limited toxicity,[5,6] finding use as MRI contrast reagents,[7,8] biomolecule tags,[9,10] and in targeted hypothermia treatments[7] and drug delivery. Magnetite also sees uses in areas such as in ferrofluids for seals and oscillation dampening.[11,12] Among different forms of iron oxides, particles of magnetite (Fe_3O_4, formally FeO: Fe_2O_3) have seen emphasis in such applications.

Here, we prepare magnetite nanoparticles in the 4−5 nm diameter range and find that they are soluble in aqueous citrate buffer solutions. The nanoparticle solution transport is controlled by diffusion as demonstrated in potential step and linear sweep experiments. Voltammetry by rotated disk voltammetry shows two electrochemically irreversible waves, well-separated (ca. 0.3 V) on the potential axis, corresponding to two different Fe(III/II) reactions of the nanoparticles. The solution voltammetry is unusual in that the Fe_3O_4 magnetite nanoparticles exhibit reactions that are both formally Fe(II) → Fe (III) and Fe(III) → Fe(II) but with different apparent formal potentials, reflecting chemically different sites in the nanoparticles. While the electrochemistry of iron oxides as films on surfaces (e.g., corrosion) has been extensively investigated,[13] this is the first report on the voltammetry of freely diffusing nanometer scale Fe_3O_4 nanoparticles.

Iron oxide nanoparticles used in biological application are desirably smaller than *ca.* 20 nm (dia.) with a modest size dispersity (typically <10%),[14] which generally improves reproducibility in sensitive measurements. These small nanoparticles are commonly prepared by aqueous coprecipitation of $Fe^{II}Cl_2$ and $Fe^{III}Cl_3$ salt mixtures in the presence of a base such as NaOH or NH_3,[8,15−17] by hydrothermal reactions,[18,19] or by electrochemical generation from sacrificial iron electrodes.[20,21] Controlling the average size and dispersity of <20 nm iron oxide nanoparticles prepared using these approaches can be difficult. An alternative pathway (used here) relies on a nonaqueous high temperature thermal degradation reaction (often >260 °C) of an iron acetate or acetylacetonate salt in media of long chain compounds such as oleylamine and/or oleic acid. This procedure, although ungainly, reproducibly yields nanoparticle batches with a modestly constrained size distribution (diameter variability ca. 10%) and bearing a fatty surfactant coating that stabilizes the nanoparticles and prevents their aggregation. Control between spherical and cubic nanoparticle morphologies has even been demonstrated with this method.[22] A general size-controlled version was described by Sun et al.[23] Additional metal acetylacetonates (such as those of Co, Ni, Mn) can be doped into the nanoparticles to manipulate their magnetism.[24]

The above high temperature thermal degradation synthesis brings the complication that their fatty capping shell makes them quite hydrophobic. The fatty capping shell can be replaced with hydrophilic reagents based on organosilanes,[8,11,17,25−29] carboxylic acids,[30] or phosphates.[31,32] The organosilanes interact covalently with the nanoparticle surfaces and by strong chemisorption in the case of carboxylic acids and phosphates.[33] These capping reagents can have specific functionalities that permit further modifications via coupling reactions (carbodiimide,[16,34] acyl chloride,[35] or click[7,32,36,37] to mention a few) to adjust solubility and can thereby produce a wide variety of nanoparticle surface chemistries.

In contrast to their technological significance,[1−13] very little is known about the electrochemistry of freely diffusing

Received: June 3, 2014
Published: July 21, 2014

   dx.doi.org/10.1021/ja505562p | J. Am. Chem. Soc. 2014, 136, 10783−10789

magnetite nanoparticles. Most prior electrochemical studies have been of bulk iron oxide materials[38] or of hematite (Fe_2O_3) nanoparticles.[39] Marken et al.[40] sought the electrochemistry of freely diffusing 4−5 nm hematite nanoparticles; while hampered by adsorption effects, with the aid of ultrasonically enhanced transport they showed a pH dependent reduction of the nanoparticles and a subsequent stripping response of electrochemically formed $FePO_4$. Other electrochemical studies of hematite nanoparticles have evaluated their potential as capacitors, with the nanoparticles being pressed into electrodes.[19]

Magnetite as a bulk material does show electrochemistry in low pH solutions, with anodic and cathodic reactions that have been formulated as[38]

$$3[Fe^{2+}Fe_2^{3+}]O_4 \rightarrow 4[Fe_2^{3+}]O_3 + Fe^{2+} + 2e^- \quad (1)$$

$$[Fe^{2+}Fe_2^{3+}]O_4 + 8H^+ + 2e^- \rightarrow 3Fe^{2+} + 4H_2O \quad (2)$$

Magnetite nanoparticles have also seen evaluation in electrode mixtures for battery applications.[18]

The nanoparticles produced by thermal degradation synthesis are coated with surfactant layers that leave them nonaqueous soluble, but the surfactant films tend to act as barriers for electron transfers to/from them. In the present work, the surfactant layer is replaced by more manageable citrate ligands so as to permit study of the diffusion-controlled nanoparticle voltammetry in pH 2 citrate buffer with added $NaClO_4$ electrolyte. The nanoparticles have an average diameter of 4.4 ± 0.9 nm, containing on averge ca. 30 Fe sites. Nanoparticle solutions display an electrochemically irreversible oxidation with E_{PEAK} at ca. +0.52 V and an irreversible reduction with E_{PEAK} at ca. +0.2 V vs Ag/AgCl. These processes are presumed to correspond to the formal potentials for one-electron oxidation of Fe(II) and reduction of Fe(III) at their different sites in the magnetite nanoparticle structure.

EXPERIMENTAL SECTION

Chemicals. Iron(III) acetylacetonate ($Fe(acac)_3$; 97%), iron(III) citrate ($C_6H_5FeO_7$; technical grade), oleylamine ($C_9H_{18} = C_9H_{17}NH_2$; 80−90%), oleic acid ($C_9H_{18} = C_8H_{15}COOH$; 97%), 1,2-hexadecanediol ($CH_3(CH_2)_{13}CHOHCH_2OH$; 90%), diphenyl ether ($(C_6H_5)_2O$; >99%), and sodium perchlorate ($NaClO_4$; >98%) were purchased from Sigma-Aldrich. Absolute ethanol, *N*,*N*-dimethylformamide (DMF), hexanes, and toluene obtained from Fisher Scientific were dried over 4 A molecular sieves.

Instrumental. The prepared magnetite nanoparticles were imaged by transmission electron microscopy (TEM; JEOL 2010F and Hitachi 9500). Energy dispersive X-ray (EDS) analysis was performed using an Oxford INCA Energy TEM 250 TEM microanalysis system attached to the JEOL 2010F. XRD data were taken on a Rigaku Multiflex powder diffractometer with Cu Kα radiation. XPS data were taken on a Kratos Axis Ultra DLD system with a monochromatic Al Kα X-ray source. High resolution scans were taken at a pass energy of 20 eV; the energy axis was aligned at the C 1s peak at 284.6 eV. Electrochemistry in solutions of pH 2.2 citrate buffer with added 1 M $NaClO_4$ electrolyte was performed at Pt working (0.02 cm^2 stationary disk, 0.196 cm^2 for rotating disk) electrodes, with Pt wire auxiliary and Ag/AgCl reference electrodes, using a CH Instruments Model CHI660a and CHI760c with a Pine Instruments rotator (Model AFMSRCE). Isolation of nanoparticles was done at 5000−6000 rpm for 10 min using an Eppendorf 5810 centrifuge with fixed-angle rotator. A CAL 9500P programmable process controller provided temperature control during nanoparticle synthesis.

Synthesis of 4 nm Diam. Magnetite Nanoparticles. The procedure used was similar to that of a previous report.[24] Measures of 0.49 g of $Fe(acac)_3$ (2 mmol), 1.5 mL of oleic acid (6 mmol), 1.3 mL of oleylamine (6 mmol), and 2.58 g of 1,2-hexadecanediol (10 mmol) were added to 20 mL of diphenyl ether in a round-bottom flask equipped with a magnetic stir bar, thermocouple, and condenser. Using a 100 mL heating mantle and sand packing to promote even heating, the vessel and contents were argon purged and heated for 30 min at 200 °C with vigorous stirring. The temperature was then rapidly increased to 265 °C; the solution color changed from dark red to black, signaling formation of magnetite nanoparticles. The reaction mixture was refluxed at 265 °C for 1 h and allowed to cool to room temperature. The black suspension was transferred to centrifugation tubes, and absolute ethanol was added to precipitate the nanoparticles which were collected by centrifugation at 6000 rpm for 10 min. This process was repeated three times to wash the nanoparticles, which were then taken up into 10 mL of hexanes solvent and stored at room temperature. The nanoparticles produced had an average diameter of 4.4 ± 0.9 nm, as shown in the TEM image and histogram of Figure 1.

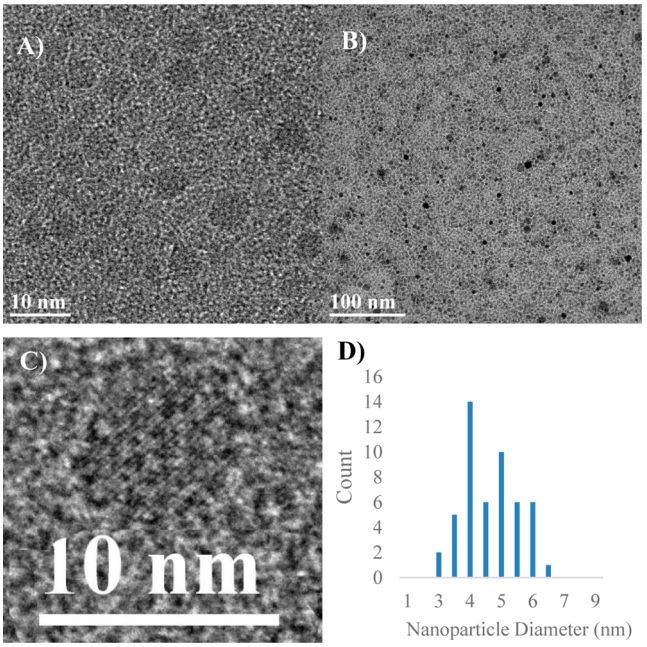

Figure 1. TEM images of as-synthesized magnetite nanoparticles. Scale bar: (A) 10 nm; (B) 100 nm. (C) Image shows lattice lines of an individual nanoparticle; (D) a histogram of magnetite nanoparticle diameters (n = 100) indicating an average diameter of 4.4 ± 0.9 nm.

Citrate Capped Magnetite Nanoparticles. In a procedure modified from Drofenik et al.,[41] 1 mL of the hexane solution of nanoparticles was rotovapped to dryness and the nanoparticles weighed (~5 mg) and redissolved in 7.5 mL of toluene in a scintillation vial. The toluene solution was added to a solution of citric acid (3 mmol, ~0.6 g) in 7.5 mL of DMF (e.g., 5 mg citric acid per 5 mg magnetite NPs) which became turbid brown. The mixture was stirred vigorously at 100 °C for 24 h and then was transferred to 50 mL centrifuge tubes, and the nanoparticles precipitated by adding diethyl ether. They were collected via centrifugation at 6000 rpm for 10 min. The brownish nanoparticle precipitate was washed twice more with fresh diethyl ether and then suspended in 15 mL of pH 2.2 citrate buffer; after 24 h this yields a homogeneous, yellow solution.

RESULTS AND DISCUSSION

Fe_3O_4 Nanoparticle Synthesis and Characterization. The produced Fe_3O_4 nanoparticles are 4.4 ± 0.9 nm in diameter and readily dissolve in nonpolar solvents (hexanes,

dx.doi.org/10.1021/ja505562p | J. Am. Chem. Soc. 2014, 136, 10783−10789

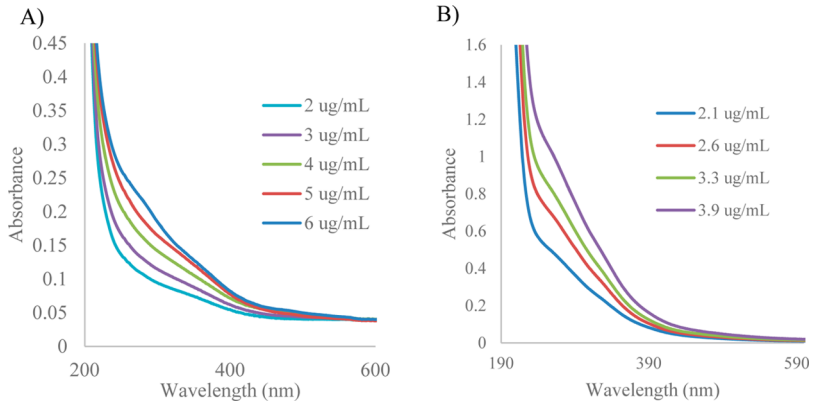

Figure 2. UV/vis spectra showing (A) the effect of serial dilution of a solution of 6 μg/mL magnetite nanoparticles in hexanes solvent and (B) the effect of serial dilution of a solution of 3.9 μg/mL Cit Fe_3O_4 in water.

toluene, chloroform), forming black solutions that are brownish when highly diluted. At high concentrations they display ferrofluidic behavior (*vide infra*). The nonpolar character of the nanoparticles is attributable to their fatty surfactant coating, which prevents aggregation and flocculation. In TEM images, the nanoparticles (Figure 1) show lattice lines indicating their crystalline nature. The lattice is spaced by ~3 Å, corresponding to (220) planes in spinel-structured magnetite.[24] The poorly resolved peaks in X-ray powder diffraction (XRD) of the nanoparticles (Figure SI-1) are consistent with previously reported data,[41] particularly the major reflection at ca. 36° (311). The UV/vis spectra of these nanoparticle solutions show strong absorbance in the UV, with several small shoulders at 275, 346, and 480 nm (Figure 2A). Molar absorptivities, expressed in terms of nanoparticle concentration and iron concentration, are listed in Table 1. Optical excitation at 350 nm results in emission peaks at 400 and 425 nm and a shoulder at ca. 450 nm (Figure SI-2). The XPS spectrum of the nanoparticles (Figure SI-3) is nearly featureless and shows only a strong C 1s peak owing to the dominating surfactant coating, as seen previously for ITO nanoparticles.[35] Attempts at observing the electrochemistry of the as-synthesized nanoparticles dispersed in an aqueous electrolyte revealed no obvious voltammetric peaks, a result probably reflecting the action of the insulating surfactant coating on the nanoparticles as a barrier to electron transfers.

Table 1. Molar absorptivities for Fe_3O_4 and Cit Fe_3O_4 in Terms of Nanoparticle (Np) and Iron Concentrations

sample name	λ (nm)	ε (cm^{-1} (Np) M^{-1})	ε (cm^{-1} (Fe) M^{-1})
Fe_3O_4	275	4.99×10^5	2220
Cit Fe_3O_4	270	4.82×10^6	21 600

Surfactant Replacement. In order to electrochemically access the nanoparticle core, the surfactant coating must be replaced. Carboxylic acids and phosphates are known to interact with metal oxide surfaces and to bind to large magnetite particles.[33] Citric acid was found to be a more convenient capping agent; capping with phosphoric acid is illustrated in Figure SI-4.

The citrate capped nanoparticles (abbrev. Cit Fe_3O_4) form a stable, cloudy red-brown suspension immediately after ligand replacement. (Like as-synthesized magnetite nanoparticles, they respond (*vide infra*) to the presence of a magnetic field.) For electrochemical experiments, the suspension was adjusted to pH 2.2 using citric acid; after 24 h, it becomes a yellow, fully dispersed solution. TEM images (Figure 3) show no change in the size of the nanoparticles after citrate capping. A small amount of flocculation often occurs in the handling of the nanoparticle samples. The absorbance spectrum of the Cit Fe_3O_4 shows a significant decrease in the number of shoulders

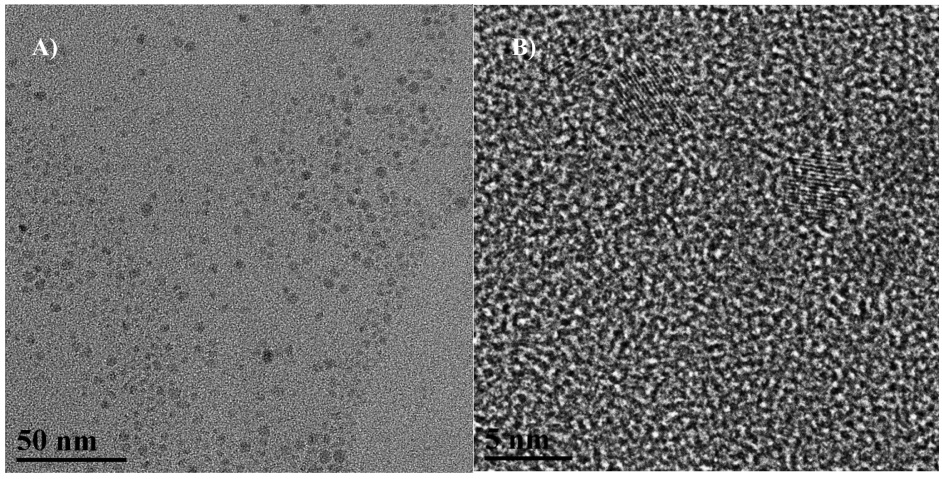

Figure 3. TEM images of Cit Fe_3O_4 nanoparticles. Scale bar: (A) 50 nm; (B) 5 nm. Panel B shows lattice lines of an individual nanoparticle.

dx.doi.org/10.1021/ja505562p | J. Am. Chem. Soc. 2014, 136, 10783−10789

and the appearance of a very broad shoulder at ca. 270 nm (Figure 2B). Molar absorptivities are presented in Table 1. Cit Fe_3O_4 nanoparticles do not show the photoluminescence seen for the as-synthesized nanoparticles; whether this is traceable to the surfactant coating was not ascertained. The XPS spectrum (Figure 4) now shows a less prominent C 1s peak (due to the thinning or removal of the surfactant layer) and a doublet of peaks corresponding to the Fe 2p photoelectrons at 709 and 722 eV.

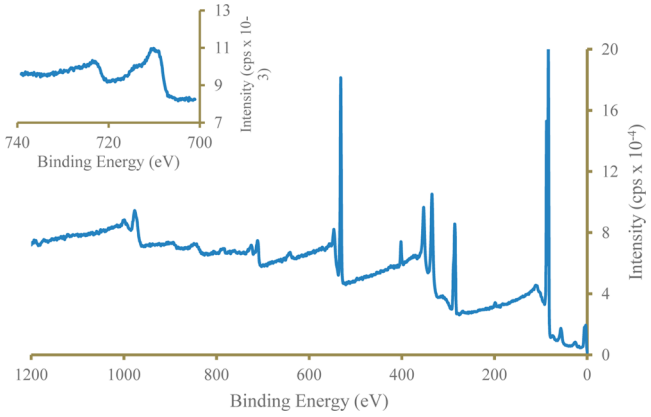

Figure 4. XPS of citrate-capped magnetite nanoparticles. Inset depicts the Fe 2P region.

Electrochemistry of Solutions of Citrate-Capped Magnetite Nanoparticles. Voltammetry of the Cit Fe_3O_4 nanoparticles was carried out in degassed pH 2.2 citric acid buffer with added 1 M $NaClO_4$ electrolyte. Both an oxidation and a reduction wave are seen following background current subtraction (Figure 5). These two voltammetric features are

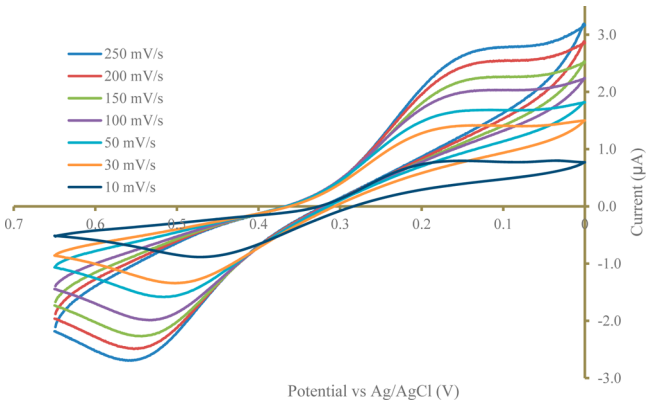

Figure 5. Background-subtracted cyclic voltammetry of 12 mM citrate capped magnetite nanoparticle solution in pH 2.2 citrate buffer, with added 1 M $NaClO_4$ electrolyte, at varying potential scan rates.

not a single redox process with a large peak splitting but rather represent different reactions, an irreversible oxidation process with E_{PEAK} *ca.* 0.52 V and an irreversible reduction process with E_{PEAK} *ca.* 0.13 V. Note that the open circuit solution rest potential (ca. 0.36 vs Ag/AgCl) lies between the two waves, consistent with the presence of both Fe(III) nanoparticle sites and Fe(II) nanoparticle sites in the solution, as expected for electrode reactions of Fe_3O_4 magnetite nanoparticles.

The Cit Fe_3O_4 cyclic voltammetry is similar to that of an Fe(III) citrate standard under the same electrochemical conditions (SI-7), though the Fe(III) citrate rest potential was further positive (ca. 0.47 V) due to the dominance of the Fe(III) form. We conclude that Cit Fe_3O_4 cyclic voltammetry is not simply that of Fe(III) citrate.

Although decidedly irreversible, the magnetite nanoparticle oxidation wave at pH 2.2 is well-defined on Pt electrodes. Observation of the reduction wave is complicated by overlap with reduction of the film of PtO_2 formed in the oxidation scan (SI-7). Background subtraction was used to eliminate the PtO_2 overlap and simplify the investigation of the redox moiety. The buffer pH is a significant parameter in the electrochemistry of the Cit FeO nanoparticles (Figures 5 and 6). At pH > 2.2, the

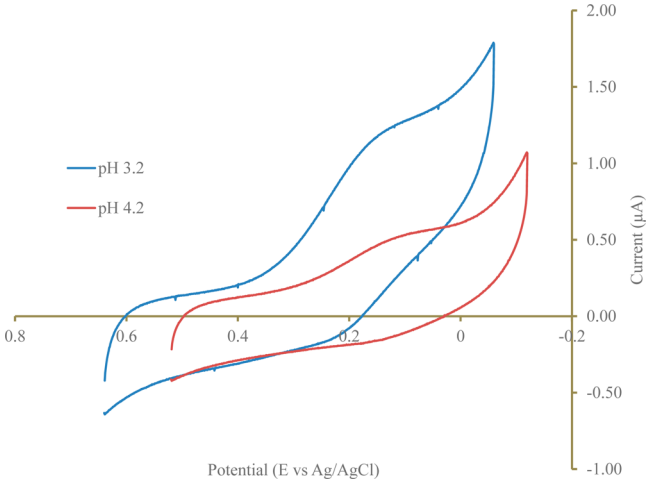

Figure 6. pH effect on cyclic voltammetry of 215 μM citrate capped magnetite nanoparticles in citrate buffer with added 1 M $NaClO_4$ electrolyte.

nanoparticle oxidation wave is no longer observed, and at pH > 4 the irreversible reduction wave has decreased almost to background current levels. Characterization of pH dependence of the magnetite nanoparticle voltammetry was accordingly constrained.

Bulk electrolysis (BE) was used to determine the formal concentration of Fe(III) sites in solutions of Cit Fe_3O_4 nanoparticles in pH 2.2 citrate buffer with 1 M $NaClO_4$, for use in calculating diffusion coefficients. These experiments were very slow, taking ca. 1−2 h for complete (99%) electrolysis. A similarly slow time frame was observed for the BE of solutions of Fe(III) citrate under similar conditions. This sluggishness is possibly due to a combination of insufficiently cathodic applied potential and slow electron transfer kinetics.

The nanoparticle electrochemistry was examined by rotating disk voltammetry (RDE) and after background subtraction gives Figure 7, which was taken in a 5 mM solution of the Cit Fe_3O_4 nanoparticles in pH 2.20 citrate buffer with 1 M $NaClO_4$ electrolyte. Limiting currents taken between potentials at 0.43 V and the oxidation plateau at 0.80 V follow (Figure 8) the Levich equation's[42] predicted [rotation rate]$^{1/2}$ relationship

$$i_l = 0.62nFACD^{2/3}\omega^{1/2}\nu^{-1/6} \quad (3)$$

where F is Faraday's constant, n = 1, ω is the angular rotation rate (radians/s), and υ is the kinematic viscosity (cm^2/s). The nanoparticle diffusion coefficient obtained from this experiment is given in Table 2. For the Fe_3O_4 material, formally $Fe^{II}O{:}Fe^{III}{}_2O_3$, limiting currents for the Fe(III) → Fe(II) reduction wave should ideally be 2× those of the oxidation

dx.doi.org/10.1021/ja505562p | J. Am. Chem. Soc. 2014, 136, 10783−10789

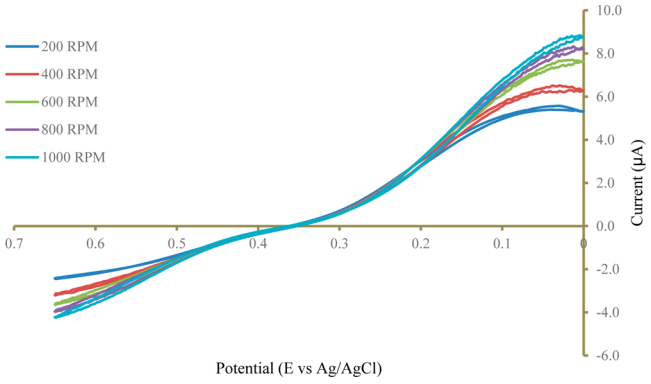

Figure 7. Background-subtracted rotating disk electrode voltammetry (potential scan rate 10 mV/s), at different rotation rates, of a 5 mM solution of citrate capped magnetite nanoparticles in pH 2.2 citrate buffer with 1 M $NaClO_4$.

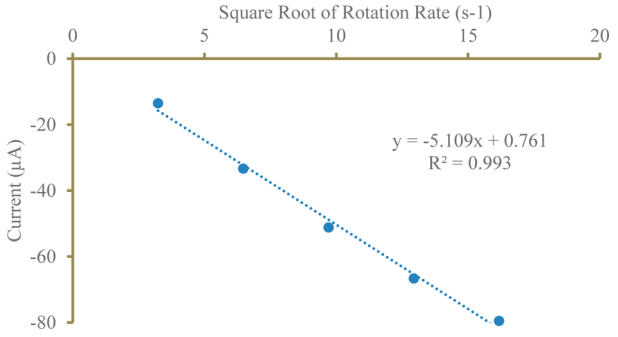

Figure 8. Levich plot of background-subtracted RDE oxidation limiting currents (values between currents at 0.43 and 0.65 V, vs Ag/AgCl) for 0.6 mM solution of citrate capped magnetite nanoparticles in pH 2.2 citrate buffer with 1 M $NaClO_4$.

Table 2. Diffusion Coefficients for Cit Fe_3O_4 Nanoparticles in pH 2.2 Citrate Buffer Solution, with 1 M $NaClO_4$

	diffusion coefficient (10^{-6} cm^2/s)
Stokes–Einstein prediction	1.1
chronoamperometry measurement	4.5 ± 2.4
rotating disk electrode measurement	1.8 ± 0.4

process. Inspection of Figure 7, comparing the limiting currents for the reduction and oxidation waves, shows indeed that is approximately the case.

In potential step chronoamperometry (CA) with steps to the reduction plateau, currents are somewhat less affected by the poor electron transfer kinetics of the system and cleanly follow the Cottrell relationship[42]

$$i(t) = nFAC\left(\frac{D}{\pi t}\right)^{1/2} \quad (4)$$

as shown in Figure 9. Its linearity supports a picture of diffusion-controlled reduction of the nanoparticles. The nanoparticle diffusion coefficients determined by these two techniques are in reasonable accord as seen in Table 2.

Plots of current vs square root of potential scan rate (Figure SI-8) further support the diffusional character of the nanoparticle electrochemical waves. The equation for linear sweep voltammetry[42] is

$$i_p = 2.99*10^5\alpha^{1/2}n^{3/2}AD^{1/2}Cv^{1/2} \quad (5)$$

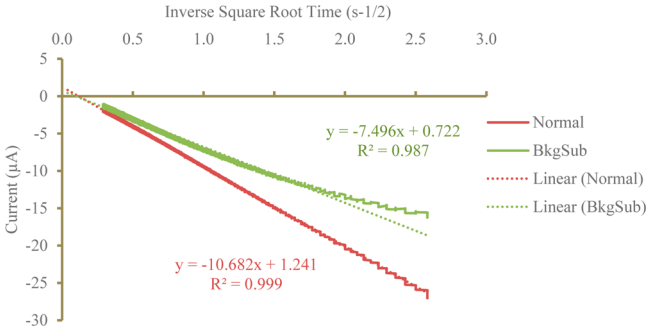

Figure 9. Cottrell plot of chronoamperometric oxidation currents over a 12 s time scale for a potential step from 0.35 to 0.70 V vs Ag/AgCl for the 5 mM solution of citrate capped magnetite nanoparticles in pH 2.20 citrate buffer with 1 M $NaClO_4$.

where n is the number of electrons delivered (one per iron site), A the area of the working electrode (cm^2), D (cm^2/s) the nanoparticle diffusion coefficient, and C (mol/cm^3) the overall concentration of active iron sites. The expected linear relation between the peak currents and the square root of potential scan rate ($v^{1/2}$) is observed, meaning again that the currents are controlled by the rate of nanoparticle diffusion. (While eq 5 is for an irreversible redox system, a $v^{1/2}$ scan rate dependency is also expected for quasi- and reversible reactions.)

Irreversible adsorption does not have an obvious role in the electrode reactions; at least no residual redox peaks are observed after moving the electrode to a fresh electrolyte solution. The results from the above data inspections using eqs 3 and 4 rule out control of the observed currents by irreversible nanoparticle adsorption on the electrode, but do not eliminate the existence of a minor amount of reversible adsorption.

A Tafel plot[42] was constructed to estimate the electrode kinetics of the two irreversible reactions of Cit Fe_3O_4 (Figure 10). Results are found in Table 3. While the reactions are being treated as two individual irreversible reactions, they have similar kinetic behavior. Transfer coefficients, α, are between 0.4–0.5 indicating the relative symmetry of the oxidation and reduction energy barriers. The standard rate constants, k^0, differ by less than a factor of 2 even though the measured rate is very slow ($k^0 = 1 \times 10^{-5}$ cm/s). For comparison, this rate constant and associated exchange current, 1×10^{-7} A/cm^2, are much smaller than that for the $Fe^{2+/3+}$ couple (exchange current ca. 1×10^{-3} A/cm^2) in aqueous and frozen conc. perchloric acid solution.[43]

Effects of Magnetic Field on Magnetite Electrochemistry. The inherent magnetism of the magnetite nanoparticles is preserved for the described materials, as shown by placing a Pt coated glass slide electrode at the bottom of a small cell (Figure SI-9). The cell was filled with a fresh (meaning prior to the 24 h aging step) pH 2.2 Cit FeO dispersion with added 1 M $NaClO_4$ electrolyte. CV scans were taken of the nanoparticles without any magnetic field. Then, a magnetic field was placed under the working electrode to draw the magnetite nanoparticles to its surface. This showed no effect for several cyclical potential scans, but after ~1 min a significant accumulation of nanoparticles could be seen on the electrode surface. The change in current is most noticeable at slow potential scan rates (Figure 11). It is important to note that the fresh nanoparticle dispersion remains in solution for ca. 1 h without the external influence of a magnet.

dx.doi.org/10.1021/ja505562p | J. Am. Chem. Soc. 2014, 136, 10783–10789

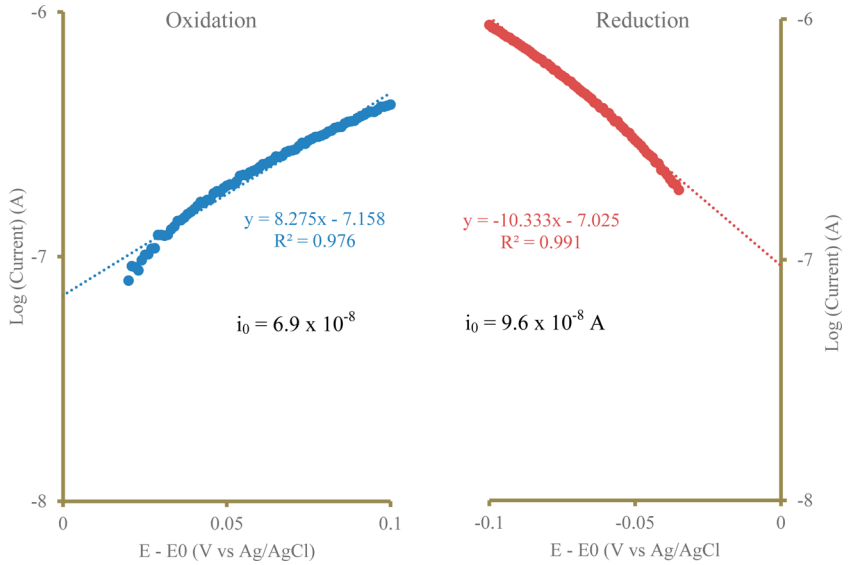

Figure 10. Tafel plots depicting the irreversible oxidation of Fe^{3+} and the irreversible reduction of Fe^{2+}. The *y*-intercept is taken to be $\log(i_0)$, where i_0 is the exchange current.

Table 3. Exchange Currents and Associated Standard Rate Constants for the Oxidation and Reduction Waves (see Figure 5) in Cit Fe_3O_4 Solutions

Cit Fe_3O_4 processes	i_0 (A)	α (mol/V)	k^0 (cm/s)
oxidation	6.9×10^{-8}	0.48	1.1×10^{-5}
reduction	9.6×10^{-8}	0.40	1.9×10^{-5}

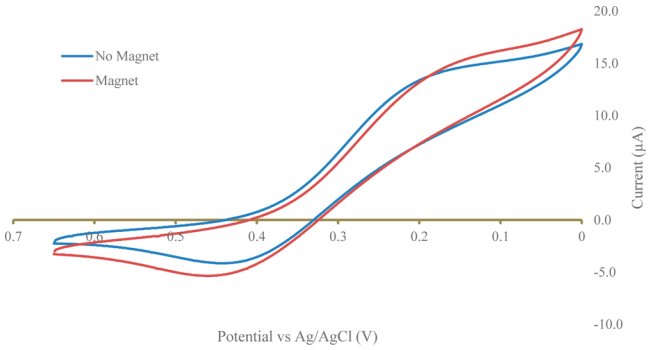

Figure 11. Cyclic voltammetry of a 12 mM solution of citrate capped magnetite nanoparticles in pH 2.2 citrate buffer with 1 M $NaClO_4$ at 30 mV/s, with (orange curve) and without (blue curve) magnetic field (see text).

SUMMARY

In conclusion, we have explored the behavior of 4 nm diameter nanoparticles which exhibit electrode reactions whereas many as 30 electron transfers occur per electrode–nanoparticle collision (plus such attendant intraparticle electron transfers as required for complete electrolytic conversion). One must assume that significant inner sphere-like effects play a role in causing the quite slow overall pace of electrode–nanoparticle electron transfers as expressed in the small electron transfer rate constants of Table 3. The overall slow pace of nanoparticle electron transfers is nonetheless sufficiently rapid to achieve a nanoparticle diffusion-controlled electrode reaction rate, as reflected in the mass transport limitations demonstrated in Figures 8 and 9. Lastly, the pattern of the nanoparticle redox voltammetry, as exemplified in Figure 5, confirms that the Fe_3O_4 nanoparticles contain two different kinds of iron sites, yet the overall electron transfer dynamics of their oxidation and reductions are similar, as shown by the data of Table 3.

ASSOCIATED CONTENT

Supporting Information

Supplementary data on nanoparticle characterization, voltammetry, and magnetic field experiment. This material is available free of charge via the Internet at http://pubs.acs.org.

AUTHOR INFORMATION

Corresponding Author

rwm@email.unc.edu

Notes

The authors declare no competing financial interest.

ACKNOWLEDGMENTS

This research was supported in part by the Office of Naval Research and the National Science Foundation. We gratefully acknowledge TEM, EDX, and XPS measurements performed by Carrie Donley and Amar Kumbhar of the Analytical and Nanofabrication Laboratory of the UNC Institute for Advanced Materials. We also acknowledge the UNC Solar Fuels and Next Generation Photovoltaics, and Energy Frontiers Research Center funded by the U.S. Department of Energy, Office of Science, Office of Basic Energy Science under Award Number DE-SC0001011, and the UNC Solar Energy Research Center Instrumentation Facility funded by the Department of Energy – Office of Energy Efficiency & Renewable Energy under Award Number DE-EE0003188.

REFERENCES

(1) Sharrock, M. P.; Bodnar, R. E. *J. Appl. Phys.* **1985**, *57*, 3919.
(2) Jung, J. H. *Chem. Soc. Rev.* **2011**, *40*, 4464.
(3) Schladt, T. D.; Schneider, K.; Schild, H.; Tremel, W. *Dalton Trans.* **2011**, *40*, 6315–6343.
(4) Yiu, H. H. P. *Nanomedicine* **2011**, *6*, 1429–1446.
(5) Shen, M.; Cai, H.; Wang, X.; Cao, X.; Li, K.; Wang, S. H.; Guo, R.; Zheng, L.; Zhang, G.; Shi, X. *Nanotechnology* **2012**, *23*, 105601.

(6) Joris, F.; Manshian, B. B.; Peynshaert, K.; De Smedt, S. C.; Braeckmans, K.; Soenen, S. J. *Chem. Soc. Rev.* **2013**, *42*, 8339−8359.
(7) Hayashi, K.; Ono, K.; Suzuki, H.; Sawada, M.; Moriya, M.; Sakamoto, W.; Yogo, T. *Chem. Mater.* **2010**, *22*, 3768−3772.
(8) Zhang, C.; Wängler, B.; Morgenstern, B.; Zentgraf, H.; Eisenhut, M.; Untenecker, H.; Krüger, R.; Huss, R.; Seliger, C.; Semmler, W.; Kiessling, F. *Langmuir* **2006**, *23*, 1427−1434.
(9) Xu, C.; Xu, K.; Gu, H.; Zheng, R.; Liu, H.; Zhang, X.; Guo, Z.; Xu, B. *J. Am. Chem. Soc.* **2004**, *126*, 9938−9939.
(10) Xie, J.; Chen, K.; Lee, H.-Y.; Xu, C.; Hsu, A. R.; Peng, S.; Chen, X.; Sun, S. *J. Am. Chem. Soc.* **2008**, *130*, 7542−7543.
(11) del Campo, A.; Sen, T.; Lellouche, J.-P.; Bruce, I. J. *J. Magn. Magn. Mater.* **2005**, *293*, 33−40.
(12) Cornell, R. M.; Schwertmann, U. *The iron oxides: structure, properties, reactions, occurrences and uses*; John Wiley & Sons: 2003.
(13) Sun, Y.-P. *Supercritical Fluid Technology in Materials Science and Engineering: Syntheses: Properties, and Applications*; CRC Press: 2002.
(14) Teja, A. S.; Koh, P.-Y. *Prog. Cryst. Growth Charact. Mater.* **2009**, *55*, 22−45.
(15) Vargas, A.; Shnitko, I.; Teleki, A.; Weyeneth, S.; Pratsinis, S. E.; Baiker, A. *Appl. Surf. Sci.* **2011**, *257*, 2861−2869.
(16) Mikhaylova, M.; Kim, D. K.; Berry, C. C.; Zagorodni, A.; Toprak, M.; Curtis, A. S. G.; Muhammed, M. *Chem. Mater.* **2004**, *16*, 2344−2354.
(17) Yamaura, M.; Camilo, R. L.; Sampaio, L. C.; Macêdo, M. A.; Nakamura, M.; Toma, H. E. *J. Magn. Magn. Mater.* **2004**, *279*, 210−217.
(18) Zhang, Z. J.; Chen, X. Y.; Wang, B. N.; Shi, C. W. *J. Cryst. Growth* **2008**, *310*, 5453−5457.
(19) Zhu, M.; Wang, Y.; Meng, D.; Qin, X.; Diao, G. *J. Phys. Chem. C* **2012**, *116*, 16276−16285.
(20) Cabrera, L.; Gutierrez, S.; Menendez, N.; Morales, M. P.; Herrasti, P. *Electrochim. Acta* **2008**, *53*, 3436−3441.
(21) Fajaroh, F.; Setyawan, H.; Widiyastuti, W.; Winardi, S. *Adv. Powder Technol.* **2012**, *23*, 328−333.
(22) Zhen, G.; Muir, B. W.; Moffat, B. A.; Harbour, P.; Murray, K. S.; Moubaraki, B.; Suzuki, K.; Madsen, I.; Agron-Olshina, N.; Waddington, L.; Mulvaney, P.; Hartley, P. G. *J. Phys. Chem. C* **2010**, *115*, 327−334.
(23) Sun, S.; Zeng, H. *J. Am. Chem. Soc.* **2002**, *124*, 8204−8205.
(24) Sun, S.; Zeng, H.; Robinson, D. B.; Raoux, S.; Rice, P. M.; Wang, S. X.; Li, G. *J. Am. Chem. Soc.* **2003**, *126*, 273−279.
(25) Barrera, C.; Herrera, A. P.; Rinaldi, C. *J. Colloid Interface Sci.* **2009**, *329*, 107−113.
(26) Bruce, I. J.; Sen, T. *Langmuir* **2005**, *21*, 7029−7035.
(27) Čampelj, S.; Makovec, D.; Drofenik, M. *J. Magn. Magn. Mater.* **2009**, *321*, 1346−1350.
(28) De Palma, R.; Peeters, S.; Van Bael, M. J.; Van den Rul, H.; Bonroy, K.; Laureyn, W.; Mullens, J.; Borghs, G.; Maes, G. *Chem. Mater.* **2007**, *19*, 1821−1831.
(29) Haensch, C.; Hoeppener, S.; Schubert, U. S. *Chem. Soc. Rev.* **2010**, *39*, 2323−2334.
(30) Harris, L. A.; Goff, J. D.; Carmichael, A. Y.; Riffle, J. S.; Harburn, J. J.; St. Pierre, T. G.; Saunders, M. *Chem. Mater.* **2003**, *15*, 1367−1377.
(31) White, M. A.; Johnson, J. A.; Koberstein, J. T.; Turro, N. J. *J. Am. Chem. Soc.* **2006**, *128*, 11356−11357.
(32) Peng, R.; Zhang, W.; Ran, Q.; Liang, C.; Jing, L.; Ye, S.; Xian, Y. *Langmuir* **2011**, *27*, 2910−2916.
(33) Neouze, M.-A.; Schubert, U. *Monatshefte für Chemie/Chemical Monthly* **2008**, *139*, 183−195.
(34) Beasley, C. A.; Murray, R. W. *Langmuir* **2009**, *25*, 10370−10375.
(35) Roberts, J. J. P.; Vuong, K. T.; Murray, R. W. *Langmuir* **2012**, *29*, 474−479.
(36) Hayashi, K.; Moriya, M.; Sakamoto, W.; Yogo, T. *Chem. Mater.* **2009**, *21*, 1318−1325.
(37) Polito, L.; Monti, D.; Caneva, E.; Delnevo, E.; Russo, G.; Prosperi, D. *Chem. Commun. (Cambridge, England)* **2008**, 621−623.
(38) White, A. F.; Peterson, M. L.; Hochella, M. F., Jr *Geochim. Cosmochim. Acta* **1994**, *58*, 1859−1875.
(39) Kijima, N.; Yoshinaga, M.; Awaka, J.; Akimoto, J. *Solid State Ionics* **2011**, *192*, 293−297.
(40) McKenzie, K. J.; Marken, F. *Pure Appl. Chem.* **2001**, *73*, 1885−1894.
(41) Campelj, S.; Makovec, D.; Drofenik, M. *J. Phys.: Condens. Matter* **2008**, *20*, 204101.
(42) Bard, A. J.; Faulkner, L. R. *Electrochemical Methods: Fundamentals and Applications*, 2nd ed.; John Wiley & Sons, Inc.: NY, 2001.
(43) Borgerding, A.; Brost, E.; Schmickler, W.; Dinan, T.; Stimming, U. *Ber. Bunsenges. Phys. Chem.* **1990**, *94*, 607−612.